Am J Transl Res 2025;17(7):5641-5653
www.ajtr.org /ISSN:1943-8141/AJTR0163504

Original Article

The importance of marginal sclerosis in the recovery of mechanical strength after curettage of bone lesions

Francisco de AS Baima Filho[1], Priscylla G Mendonça[2], Giuliano F Morgantetti[1], Alice C Silva-Sousa[3], Leonardo R Battaglion[1], Ramon SYRC Silva[4], Maria do S de S Cartagenes[2], Edgard E Engels[1]

[1]Ribeirão Preto Medical School, University of São Paulo (FMRP-USP), Ribeirão Preto, SP, Brazil; [2]Federal University of Maranhão (UFMA), Maranhão, Brazil; [3]Ribeirão Preto Dental School, University of São Paulo (FORP-USP), Ribeirão Preto, SP, Brazil; [4]University of Brasília (UNB), Brasília, Brazil

Received January 22, 2025; Accepted July 5, 2025; Epub July 25, 2025; Published July 30, 2025

Abstract: Objectives: This study investigated the role of marginal sclerosis in the recovery of mechanical strength following curettage and grafting of osseous lesions. To date, it remains unclear as to whether marginal sclerosis fully or partially restores the mechanical resistance of the affected bone to compressive, flexural, and torsional loads. Methodology: Adult male *Rattus norvegicus* rats (WISTAR albino strain) aged approximately 90-days were used. Bone defects were created in the tibiae, and the animals were subsequently euthanized at different time points for outcome analysis. Various assessment methods were employed, including radiography, histology, immunohistochemistry, microcomputed tomography (micro-CT), mechanical bending and torsion tests. Results: This study revealed a progressive thickening of the osseous window borders before complete closure and a significant correlation between the intensity of marginal sclerosis that was radiographically observed, the rate of bone formation on histology, and the newly formed bone volume on micro-CT. Radiographs revealed thin marginal sclerosis at seven days post surgery, with a significant increase in sclerosis thickness being observed at ten days, whereas micro-CT revealed proportions of new bone formation of 44.80% at seven days and 105.70% at ten days. Additionally, at seven days, the mechanical resistance of the operated bones to torsion and bending was comparable to that of the non-operated bones, thereby indicating a complete recovery of mechanical strength. Conclusion: This study revealed that the appearance of marginal sclerosis around bone defects (as identified by radiography) is associated with the complete recovery of mechanical strength in rat tibiae under both bending and torsion.

Keywords: Rat, bone sclerosis, radiography, mechanical test, microtomography

Introduction

The loss of mechanical stability in bone structures occurs in cases of macroscopic alterations in bone anatomy, often resulting from fractures or bone defects; moreover, the successful healing of a fracture is referred to as consolidation. During this process, the bone gradually regains its stiffness and strength as mineralization occurs, thereby leading to a stable and pain-free fracture site. Radiographic examinations have revealed the presence of trabecular or cortical bone, which crosses the fracture site [1, 2].

In the case of bone defects, such as those caused by surgical biopsies, bone graft harvesting, benign bone tumor curettage, and debridement of osteomyelitis, the initial natural response of the bone is not to completely fill the defect and restore its original conformation. Instead, the bone tends to elicit thickening of the walls of the defect, which is a phenomenon known as marginal sclerosis. This thickening has been identified in plain radiographs and appears to be associated with the recovery of the bone's mechanical strength. Therefore, the successful healing of a bone defect initially depends on the remodeling of the bone window.

Bone modeling and remodeling are fundamental processes for reducing the risk of fractures. Remodeling involves the renewal of bone tissue by removing old bone and forming new bone, thereby aiming to maintain the mechanical properties of the bone. In contrast, modeling refers to the addition or removal of bone tissue in

https://doi.org/10.62347/GZLN4148

response to mechanical demands, thereby adapting the bone structure to external stimuli. Both processes involve the same cell types, including osteoclasts (which are responsible for bone resorption) and osteoblasts (which are responsible for bone formation). Osteocytes, which act as mechanosensors, play critical roles in regulating the location of bone remodeling. Furthermore, the likelihood of bone formation or resorption is influenced by mechanical stimuli [3].

From a radiographical perspective, marginal sclerosis appears as a rim of dense bone that delineates the borders of the bone window or defect in the trabecular bone. However, it remains unclear as to whether this sclerosis fully or partially restores the mechanical resistance of the affected bone to compressive, bending, and torsional forces. Many benign bone tumors and pseudotumoral lesions, such as giant cell tumors of bone, enchondromas, fibrous cortical defects, and chondroblastomas [4], are treated with curettage, which can lead to bone fragility and an increased risk of fracture. To mitigate this risk, several approaches are employed, including osteosynthesis, bone defect filling, or a combination of these methods, as well as prolonged non-weight-bearing rest [4-8]. Critically, the decision regarding when to allow weight-bearing to occur on the operated limb should be made by the surgeon based on the patient's clinical evaluation, specific surgical characteristics, and overall bone condition. This careful decision-making process ensures safe and effective recovery, thereby minimizing the risk of complications such as postoperative fractures.

This study aimed to establish a relationship between the presence of marginal sclerosis in bone defects (as identified on plain radiographs) and the recovery of mechanical strength under flexural and torsional loads in a rat animal model.

Materials and methods

Study location

This study was conducted at the laboratories of the Federal University of Maranhão (UFMA) and the Ribeirão Preto Medical School of the University of São Paulo (FMRP-USP).

Animals

Adult male Wistar rats (*Rattus norvegicus*, albino variety), which were approximately 90-days-old and with an average weight of 400 g, were used in this study. During the experiment, the rats were provided with standard chow and unrestricted access to water while being maintained under strictly controlled light and temperature conditions.

Ethical considerations

This study was approved by the Animal Use Ethics Committee (CEUA) of Federal University of Maranhão (UFMA) under protocol number 23115.025741/2021-44. Animal care followed the guidelines of the Brazilian National Council for the Control of Animal Experimentation (CONCEA), including regular clinical assessments to monitor the animals' general health, anesthetic protocols, postoperative analgesia, and pain evaluation via facial expressions [9]. The study and manuscript preparation adhered to the protocols outlined in the ARRIVE Guidelines (Animal Research: Reporting of In Vivo Experiments) 2.0 (2020). The authors declare that they have no conflicts of interest related to this study.

Pilot study

This pilot study aimed to establish a timeline for the development of marginal sclerosis after tibial perforation. The study identified the earliest observable presence of sclerosis and the stage at which sclerosis was fully developed (but without new bone filling the defect). These assessments were conducted using radiographic imaging and confirmed by using histological and immunohistochemical analyses.

Four rats underwent tibial perforation on Day Zero (D0), and their tibias were collected at intervals of 4, 7, 10, and 13 days (D4, D7, D10, and D13, respectively) post surgery. The early phase (EP) marked the first appearance of marginal sclerosis and remodeling, whereas the late phase (LP) indicated well-established sclerosis without defect closure, as validated via radiographic and histological findings.

Comparative study

A total of 24 rats underwent tibial perforation of the right tibia at D0 (Day Zero). Twelve rats were

euthanized at the EP (early phase), and the remaining 12 were euthanized at the LP (late phase). Three tibias from each phase (EP and LP) were analyzed using microcomputed tomography (micro-CT). The remaining tibias underwent mechanical testing; specifically, six tibias from the EP and six tibias from the LP were subjected to flexion tests, whereas the other six tibias from each phase underwent torsion tests.

In each control group, one "with defect" (WD) tibia and one intact (I) tibia were analyzed using micro-CT before mechanical testing. Six WD and six I tibias subsequently underwent flexion testing, and the remaining six WD and six I tibias were subjected to torsion tests.

Surgical model

The surgical creation of the tibial bone window followed a detailed protocol to ensure animal welfare and reproducibility. Preanesthetic care involved a subcutaneous dose of morphine (2 mg/kg) administered 30 minutes prior to anesthesia, with anesthesia being induced with intraperitoneal injections of ketamine (60-90 mg/kg) and xylazine (6-10 mg/kg) [9]. Maintenance anesthesia was achieved with isoflurane via a face mask.

Under aseptic conditions, a medial incision was used to expose the tibia, and a 2.0 mm bone window was created at the metaphysis-diaphysis transition using a Kirschner wire in controlled motion. The surgical site was irrigated with saline and closed with 3.0 nylon sutures. Postoperative care included daily wound cleaning and analgesia administration with subcutaneous Meloxicam® (1 mg/kg/day for 72 hours) [9]. The animals were housed in groups of four and monitored daily for pain using facial expression analysis; no signs of postoperative complications or distress were observed.

Guidelines from the National Council for the Control of Animal Experimentation (CONCEA) were strictly followed, with protocols in place for managing pain and determining criteria for euthanasia [9]. All of the animals maintained limb activity without adverse effects, and no exclusions occurred due to complications.

Specimen collection

Euthanasia was conducted on specific days during the EP (early phase) or LP (late phase) (according to the experimental timeline) via an intraperitoneal injection of ketamine and xylazine at three times the standard anesthetic dose [9]. After the deaths of the animals were confirmed, the operated limbs were carefully removed.

The collected specimens were wrapped in gauze moistened with 0.9% saline solution, sealed in individual containers, and stored at -23°C. Proper disposal of the animal carcasses was performed in accordance with institutional and regulatory guidelines.

Radiographic evaluation

Radiographs of the animals' limbs were obtained using a Siemens Multix B X-ray machine and captured on a digital cassette (Kodak-View, 24 × 30 cm). The imaging parameters included a focus-film distance of 85 cm, an exposure time of 0.8 seconds, a potential difference of 45 kV, and an amperage of 50 mA. The images were digitally processed.

Histological evaluation

Extracted tibias were fixed in 10% formalin for 24 hours before being decalcified in a solution for 15 days. Following decalcification, the samples were processed for histological analysis and embedded in paraffin.

Longitudinal sections of the tibial samples were prepared and stained with hematoxylin-eosin (H&E) for routine analysis. Sections were cut at three different depths using a microtome with a steel blade, with a thickness of 4 µm per section being obtained. The most representative sections of the bone defect were selected for further evaluation.

Immunohistochemical evaluation

High-quality histological sections from four samples were selected for immunohistochemical analysis. The slides were initially immersed in xylene to dissolve the mounting medium, and the coverslips were removed. After bleaching with sodium hypochlorite and rinsing, Leica Acrytol mounting medium was reapplied, and the fragments were transferred to silanized slides.

Three slides per sample were prepared for immunohistochemistry using the markers Ki-

67, SATB2 (Special AT-rich sequence-binding protein 2), and calcitonin, with two fragments being utilized per slide. Tissue hydration and antigen retrieval were performed using the Agilent Dako PTLink system with the EnVision FLEX High pH Kit. Automated processing was completed using the Dako Agilent Autostainer and the appropriate reagents.

Utilized antibodies and specifications: SATB2: Clone EP281 (Cell Marque); Calcitonin: Polyclonal (Dako); Ki-67: Clone MIB-1 (Dako).

The final steps included dehydration via alcohol and xylene immersions, with coverslips being mounted by using Leica CV5030 equipment.

Microcomputed tomography (Micro-CT)

Bone samples were scanned using a SkyScan 1174 micro-CT scanner utilizing the following conditions: 50 kV voltage, 800 mA current, 19.65 μm resolution, and a 0.5 mm aluminum filter. The samples were stabilized in test tubes during a 40-minute scan that captured 360° rotations with 1° increments. The data were saved as TIFF (Tagged Image File Format) files and reconstructed into axial sections using NRecon software.

Quantitative analysis of new bone volume was conducted with CTAn software. Images were segmented using Otsu's method, followed by 3D analysis using voxel-based processing. Unlike the less precise 2D pixel-counting method, the 3D approach provides accurate spatial measurements, including bone surface (BS), bone volume (BV), and total volume (TV) measurements, thus reflecting the sample's morphology. This method ensures reliable quantification and better representation of biological structures [10].

Mechanical testing protocol

Destructive mechanical tests, including flexural and torsional testing, were performed until the tibial specimens were fractured. Bones were stored at -23°C and transitioned to testing temperatures in a stepwise manner: 24 hours at 3°C, followed by 2 hours at room temperature to achieve thermal equilibrium.

Before testing, each tibia was measured for weight, length, and diameter at the region of the drilled bone window. These measurements ensured consistency in the testing conditions and allowed for a detailed analysis of the mechanical properties.

Flexural testing procedure: The flexural testing was conducted using an EMIC DL 10000 universal testing machine under three-point loading conditions. A span of 25 mm and a deformation rate of 1 mm/min were applied. Force measurements were captured by a 1960 N load cell, and deformations were tracked with a centesimal dial gauge.

Preloading of 3 N for 20 seconds was applied for stabilization. The tibiae were consistently oriented, with the drilled window facing upward near the right support. Manual placement ensured proper positioning, even though initial instability was observed until the load cell became stabilized. Force was then applied to the convex region of the tibia. Prior studies have indicated no significant mechanical differences between applications of force to the convex or concave portions of the bone [11].

Torsional mechanical testing procedure: Torsional mechanical testing involved embedding both ends of each tibia in acrylic cement to ensure stability during the test. Each end was secured in a 1 cm^3 mold, and care was taken to leave the bone window exposed for proper machine fixation. This preparation step reduced the free span of the bone by 2 cm.

The embedded specimens were stored at 3°C and brought to room temperature two hours before testing. Testing was performed using an INSTRON 55MT machine, with the twisting speed set to 30° per minute. The free span (defined as the length of the bone available for torsion) was measured after fixation to the machine. This setup ensured the consistent and accurate application of torsional force.

Results analysis

Quantitative data were analyzed by calculating the means and standard deviations, whereas qualitative variables were expressed as percentages. Comparisons of the means between groups regarding the mechanical testing were performed using a one-tailed Student's t test for independent samples to determine significant differences. For the microcomputed to

mography (micro-CT) evaluations, the percentage of new bone formation was used to compare the experimental groups. A *P* value of less than 0.05 was considered to be statistically significant. All of the statistical analyses were conducted using Microsoft Excel®.

Results

Pilot group

Macroscopic results: Macroscopic observations revealed a dynamic progression of bone healing across different time points (**Figure 1**).

Day 0 (Euthanasia): The bone defect was clearly visible and resembled the characteristics noted after four days, thus suggesting minimal changes and representing the early healing stage.

Day 4: The defect maintained its initial appearance, thereby indicating stability in the bone defect during this period.

Day 7: Visible new bone formation marked the beginning of regeneration, although the defect had not yet closed.

Day 10: Sclerosis became evident along the defect walls, thus signifying an organized and robust healing response.

Day 13: Substantial new bone was present around the defect, thus indicating significant regeneration progress. Despite these advancements, the structure of the bone remained distinct from its intact state, thereby reflecting permanent changes induced by the surgical process.

Radiographic results: Radiographic analysis revealed distinct healing stages across the time points (**Figure 2**).

Day 4 (D4): The bone defect remained visible with no notable changes, which is consistent with the typical postoperative appearance of the surgical area.

Day 7 (D7): The defect diameter was unchanged from D4; however, a thin sclerosis halo was evident around the bone window, thus marking the early stages of the healing process.

Day 10 (D10): A more pronounced sclerosis halo was observed around the defect, thereby indicating increased biological activity and new bone formation.

Day 13 (D13): Substantial new bone formation was evident around the bone window, which indicated advanced regeneration and the effectiveness of the repair process over time.

Histological results: Histological analysis of the bone defect revealed distinct phases of healing at each time point (**Figure 3**).

Day 4 (D4): The surgical defect was visible without a bony bridge. The defect area predominantly contained fibrin, which is characteristic of the early healing phase, with no evidence of bone tissue formation.

Day 7 (D7): Newly formed osteoids with sparse calcification began forming a bridge across the defect. Increased osteoblastic activity (which was evident based on the abundance of osteoblasts in the region) marked the onset of mineralization and bone regeneration.

Day 10 (D10): The osteoid bridge was completely formed and diffusely calcified. The presence of osteoblasts and fibroblasts indicated active cellular participation in advancing the healing process.

Day 13 (D13): A thick, fully calcified osteoid bridge with a cotton-like pattern was observed. Exuberant osteoblastic activity extended to the subperiosteal region, and signs of endochondral ossification were evident. The medullary canal was nearly obliterated, thereby reflecting an advanced stage of bone regeneration and remodeling.

Immunohistochemistry results: Calcitonin (**Figure 4**): Images from Day 4 (D4), Day 7 (D7), and Day 10 (D10) were negative for calcitonin, as no osteoclasts were identified in the histological analysis. This result aligns with the exclusive observation of new tissue formation during these periods. No data for D13 were available because of tissue detachment that occurred during slide processing.

Ki-67 (**Figure 5**): Positive staining was detected for hematopoietic cells on D4, D7, and D10. This result reflects active cell proliferation in the tissue. As with calcitonin, no D13 data were available due to tissue detachment.

Figure 1. A. Bone within the osseous window immediately after the rats were euthanized (Day 0). B. Hole with 4 days of progression exhibiting no new bone formation. C. Hole with 7 days of progression exhibiting new bone formation within the osseous window, although it was not fully closed. D. Hole with 10 days of progression displaying complete closure and sclerosis formation around the hole. E. Hole with 13 days of progression exhibiting significant new bone formation both within and surrounding the bone defect. F. Intact bone collected after the rats were euthanized, which demonstrated that the bone did not return to its original state.

Figure 2. X-rays of the tibias from the pilot group rats, with euthanasia performed at 4 days (A), 7 days (B), 10 days (C), and 13 days (D). The red markings indicate the locations of the bone defects. Even at Day 13, the hole was not occluded with new bone and exhibited a substantial degree of sclerosis.

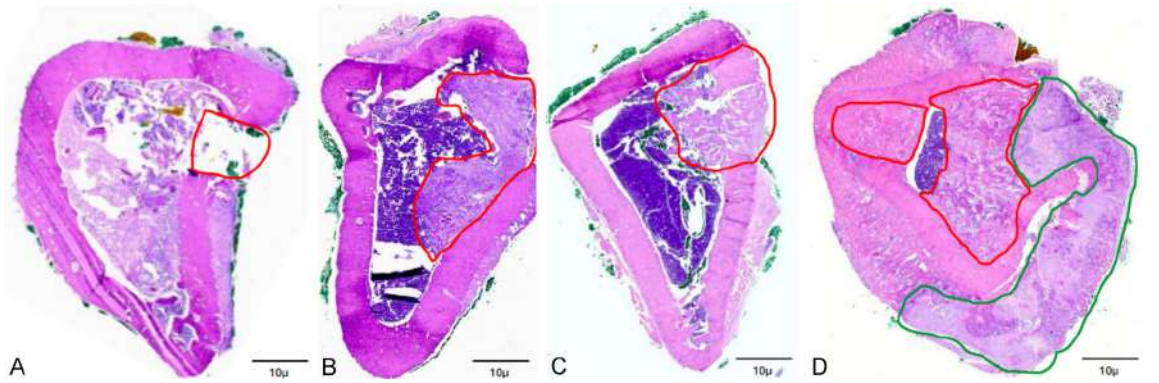

Figure 3. Histological sections stained with hematoxylin-eosin (H&E) at 40× magnification corresponding to the pilot group at different days after the creation of the bone defect. The defect area predominantly contained fibrin is observed at Day 4 (A), sparse calcification is observed at Day 7 (B), a diffusely calcified bridge with the presence of fibroblasts is observed at Day 10 (C), and a fully calcified bridge with a cotton-like pattern (as well as an almost complete disappearance of the medullary canal) is observed at Day 13 (D).

SATB2 (**Figure 6**): Positive staining was observed in the bone tissue across all of the time points (D4, D7, D10, and D13). Although a quantitative analysis was not performed, a visible increase in the reagent concentration was evident from D4 to D13, thus suggesting that progressive expression was associated with bone regeneration.

Decision regarding study groups: This study aimed to assess the mechanical strength of sclerosis adjacent to bone defects compared with that of intact bone, with a focus on healing adaptations occurring after the generation of the defects. Based on the findings, two euthanasia dates at seven days (Group A) and ten days (Group B) were selected to represent distinct stages of bone healing.

Group A (GA): Euthanasia at 7 days. Radiographic findings indicated a small, uniform sclerosis area nearly encircling the defect. Histological analysis revealed a newly formed osteoid bridge with sparse calcification, which represented an early healing phase in which sclerosis was developing but bone tissue maturation remained incomplete.

Group B (GB): Euthanasia at 10 days. Radiographs revealed well-defined, thicker sclerosis margins compared with Group A. Histological

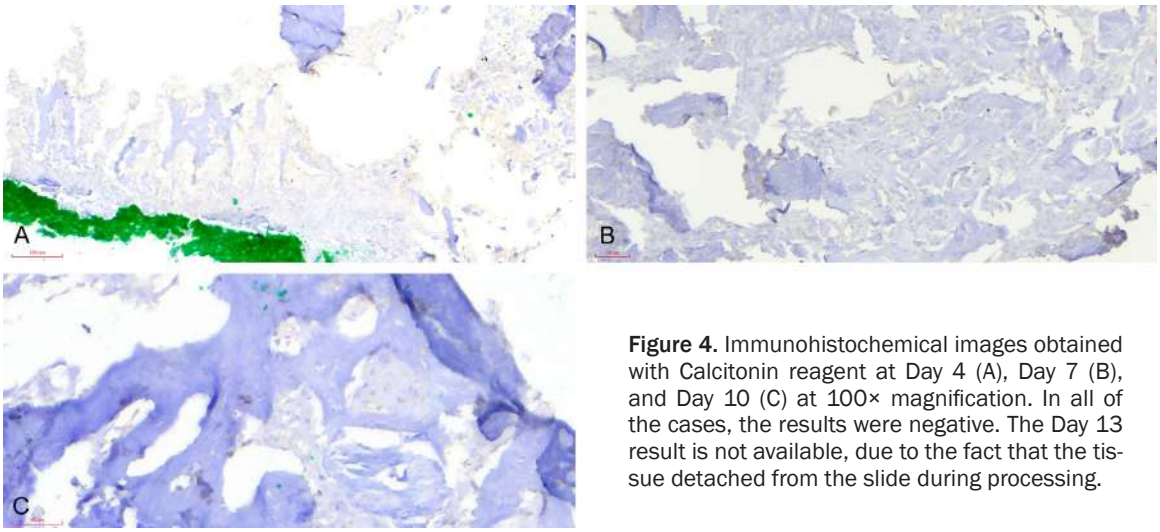

Figure 4. Immunohistochemical images obtained with Calcitonin reagent at Day 4 (A), Day 7 (B), and Day 10 (C) at 100× magnification. In all of the cases, the results were negative. The Day 13 result is not available, due to the fact that the tissue detached from the slide during processing.

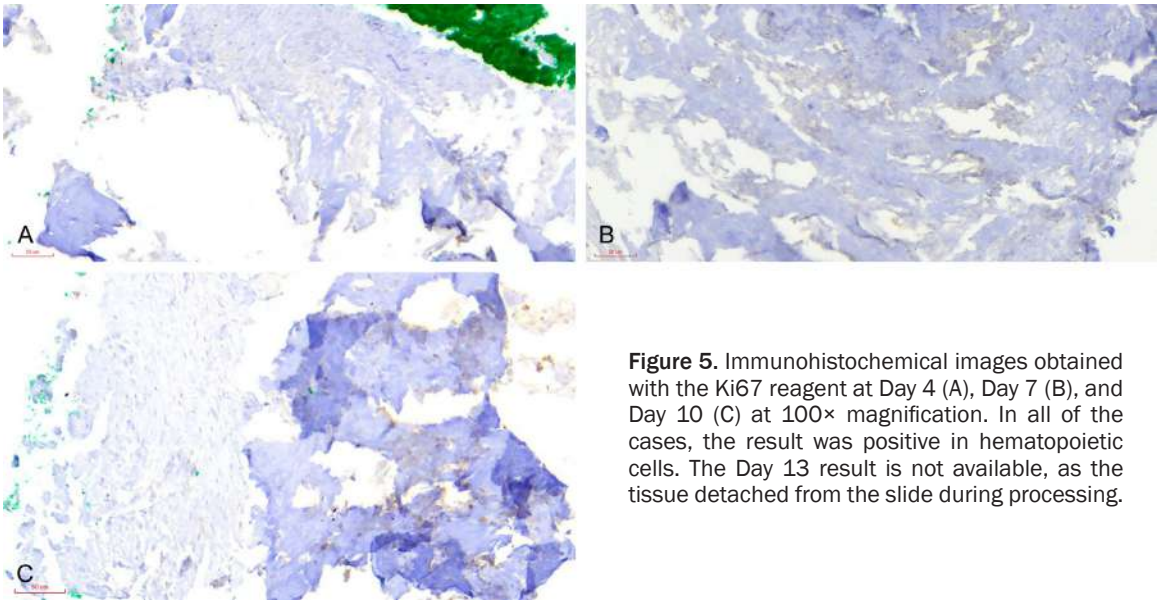

Figure 5. Immunohistochemical images obtained with the Ki67 reagent at Day 4 (A), Day 7 (B), and Day 10 (C) at 100× magnification. In all of the cases, the result was positive in hematopoietic cells. The Day 13 result is not available, as the tissue detached from the slide during processing.

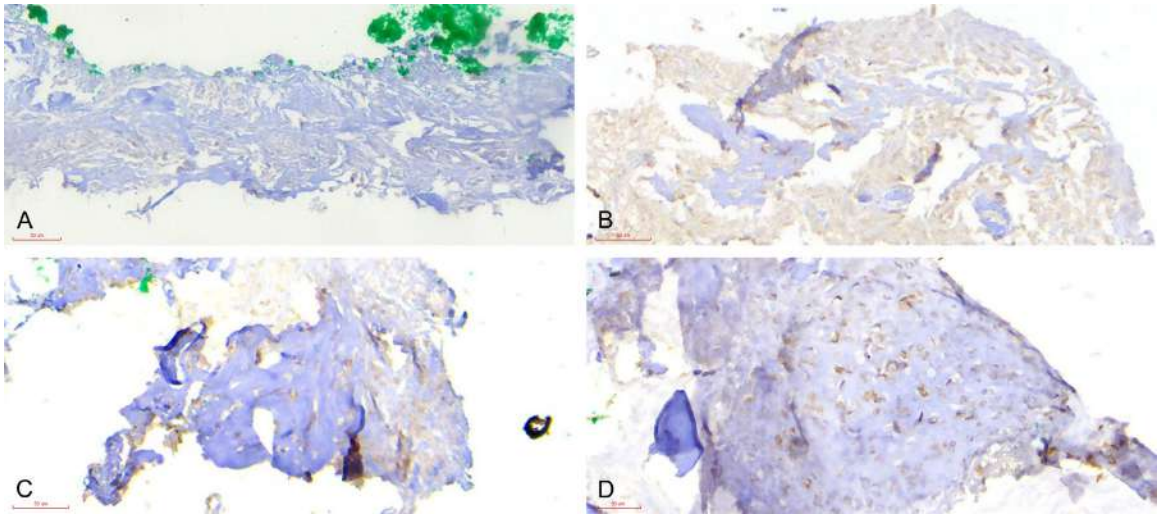

Figure 6. Positive results were observed in the bone bridges across the four study dates of Day 4 (A), Day 7 (B), Day 10 (C), and Day 13 (D) at 100× magnification. An increase in the reagent concentration over time is qualitatively evident.

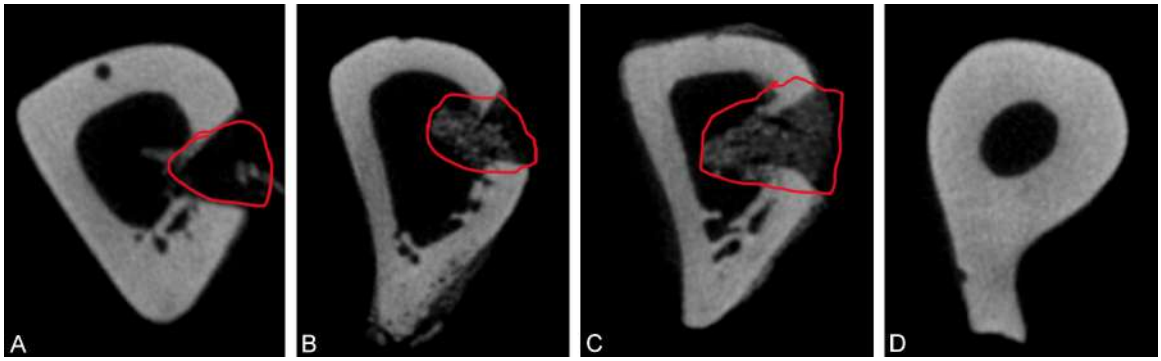

Figure 7. Microcomputed tomography (micro-CT) images from the four comparative study groups. A. "with defect" Group with 0% new bone formation. B. Group A with 44.80% new bone highlighted in red. C. Group B with 105.70% new bone highlighted in red. D. Intact Group with 100% bone.

Table 1. Bone volume-to-total volume ratio (BV/TV %) values obtained for three samples each from Group A (GA) and Group B (GB). A reference value of 0% was used for the "With Defect" Group (WD), and a value of 100% was used for the "Intact" Group (I)

RATS	BV/TV (%) RESULTS
WD	0
GA 1	24.44
GA 2	50.22
GA 3	59.71
GB 1	105.41*
GB 2	95.87
GB 3	115.73*
I	100

Note: The asterisk (*) highlights cases in Group B (GB) where the percentage of new bone formation exceeded 100%.

Table 2. Results obtained from the mechanical flexion test regarding the force (N) required to break the bone in each group

	Force (N)			
Tibia	With defect	Group A	Group B	Intact
1	84.85	71.31	90.52	65.44
2	59.59	89.89	70.89	102.18
3	80.09	83.22	83.22	80.8
4	67.56	71.07	73.47	89.07
5	62.83	75.1	96.31	83.52
6	67.58	96.85	94.18	74.22

Table 3. Results obtained from the mechanical torsion test regarding the peak torque (N.m) required to break the bone in each group

	Peak Torque (N.m)			
Tibia	With defect	Group A	Group B	Intact
1	0.2565	0.2327	0.2784	0.2155
2	0.232	0.2484	0.2655	0.2447
3	0.1812	0.2342	0.4834	0.2791
4	0.2313	0.282	0.2171	0.2364
5	0.1101	0.2701	0.2931	0.2666
6	0.1869	0.2759	0.2035	0.3292

analysis revealed an incompletely calcified bone bridge and the persistent presence of fibroblasts, thereby suggesting more advanced healing and tissue maturation stages.

Day 13 was excluded from the study groups due to the histological findings of a fully calcified bridge, absence of fibroblasts, and completion of the healing process. The inclusion of data from Day 13 would have limited the comparative analysis of the mechanical strength between different stages of healing.

Comparative study groups

Microcomputed tomography (micro-CT) test: When considering Group "with defect" (WD) with 0% new bone formation and Group "Intact"

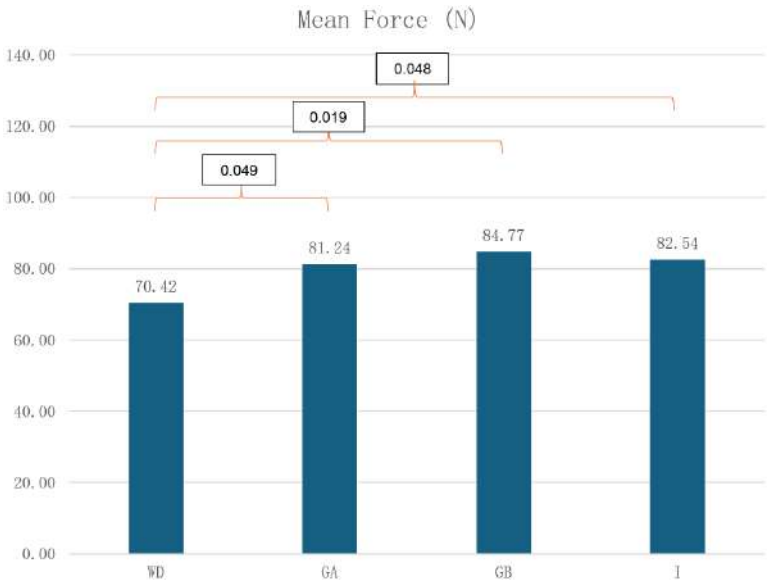

Figure 8. Bar graph displaying the mean force (N) across the groups in the mechanical flexion test. Statistically significant differences were observed in the comparisons between "with defect" Group (WD) and Group A (GA), "with defect" Group (WD) and Group B (GB), and "with defect" Group (WD) and Intact Group (I). The numbers located above the brackets indicate the *p* value.

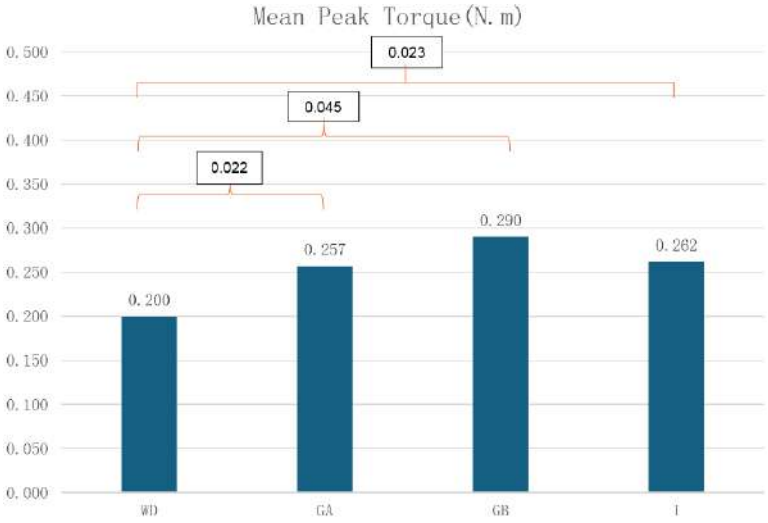

Figure 9. Bar graph displaying the mean peak torque (N.m) across the groups in the mechanical torsion test. Statistically significant differences were observed in the comparisons between "with defect" Group (WD) and Group A (GA), "with defect" Group (WD) and Group B (GB), and "with defect" Group (WD) and Intact Group (I). The numbers located above the brackets indicate the *p* value.

(I) with 100% new bone formation, new bone formation was observed to be 44.80% in Group A and 105.70% in Group B. Axial bone images from the micro-CT analysis are shown in **Figure 7**. **Table 1** presents bone volume-to-total volume ratio expressed as a percentage (BV/TV %) results for three samples from Group A and three samples from Group B.

Flexion and torsion mechanical tests: The flexion mechanical test results (expressed as force in N) for each bone are detailed in **Table 2**, whereas the torsion mechanical test results (expressed as peak torque in N·m) are shown in **Table 3**.

The flexion and torsion mechanical tests revealed statistically significant differences in the bone strength parameters between Group "with defect" (WD) and the experimental groups. For the flexion test, significant differences in force (N) were observed when Group "with defect" was compared with Group A (P=0.049), Group B (P=0.019), and Intact (P=0.048), as illustrated in **Figure 8**. Similarly, the torsion test demonstrated significant differences in peak torque (N.m) between Group "with defect" and Group A (P= 0.022), Group B (P=0.045), and Intact (P=0.023), as shown in **Figure 9**.

Discussion

The fragility caused by the curettage of bone lesions often leads surgeons to delay the initiation of weight-bearing activities on the operated limbs for patients. However, uncertainty persists regarding the appropriate timing for patients to safely resume weight-bearing activities. Beyond complete bone remodeling, no reliable parameters currently exist to determine when the risk of fracture has been fully mitigated.

Marginal sclerosis is a common finding; however, its relationship with the recovery of bone

mechanical integrity remains poorly understood. Bone defect healing typically occurs via complete closure of the defect. However, prior to closure, the thickening of the edges of the bone window (radiologically identified as marginal sclerosis) can be observed [12]. This thickening represents a response to the redistribution of mechanical stresses caused by the defect, thus leading to stress concentration at the defect edges and stimulating bone formation in this region. In this study, this type of bone formation was demonstrated via histological and microtomographic analyses.

This study also revealed that when marginal sclerosis became visible on radiographs, the volume of newly formed bone increased by 44.70% relative to the defect volume. At this stage, the mechanical strength of the bone was comparable to that of intact bone. In later analyses, before complete closure of the lesion, the volume of newly formed bone reached 105.7% of the defect volume. Both histology and microtomography demonstrated a high concentration of new bone at the defect edges, even though the defect remained open. These findings suggest that mechanical strength recovery can be achieved through structural adaptations that do not necessarily result in complete defect closure. Instead, these adaptations create a new bone structure characterized by edge thickening (rather than full defect resolution).

When considering studies correlating total callus volume with mechanical testing, three investigations reported no or minimal associations between these variables [13-15], whereas two studies identified moderate associations [16, 17]. When the total callus volume was compared with torsion testing, two studies also reported minimal or no correlation [14, 18]. In contrast, this study revealed a significant relationship between newly formed bone and the recovery of mechanical strength, as evidenced by the flexural and torsional mechanical testing results. Statistically significant differences were noted when Group A and Group B were compared with the control group (Group "with defect").

An experimental rat model was used to achieve results with potential clinical relevance [19]. The utilized 2-mm defect model was based on previous studies [4-8] and allowed for weight-bearing to occur on the operated limbs, thereby eliminating confounding factors that may influence bone remodeling [20-22].

Immunohistochemistry analysis revealed intense new bone formation between the fourth and thirteenth postoperative days, without evidence of osteoclast-mediated remodeling. SATB2 plays a critical role in bone remodeling by regulating the differentiation of mesenchymal cells into osteoblasts and promoting their maturation. Previous studies in mice have demonstrated that SATB2 deficiency leads to reduced bone mineralization, thus resulting in shortened and fragile limb bones [23-25]. The Ki-67 marker, which is a sensitive nuclear protein associated with cell proliferation, is essential for cell cycle regulation [26, 27]. Moreover, calcitonin, which is a hormone secreted by the thyroid gland, binds exclusively to osteoclast receptors and plays a role in regulating bone resorption [28].

Although these findings cannot be directly extrapolated to humans, they provide a solid foundation for future research exploring the relationship between sclerosis observed on radiographs and mechanical strength in patients. Additionally, the results offer valuable insights for clinical practice, particularly regarding procedures involving bone defects and the assessment of mechanical strength recovery.

Conclusion

In conclusion, following the curettage of bone defects, the thickening of the edges of the bone window precedes the defect's closure, which corresponds to the marginal sclerosis observed on radiographs. The utilized rat model demonstrated that when 50% of the bone defect volume is replaced with newly formed bone, marginal sclerosis becomes radiographically visible. This finding coincides with a complete recovery of mechanical strength in both flexion and torsion, thereby highlighting the potential of marginal sclerosis as a radiographic indicator of mechanical integrity recovery.

Disclosure of conflict of interest

None.

Address correspondence to: Dr. Francisco de AS Baima Filho, Bioengineering Laboratory, Av. Bandeirantes, 3900, Monte Alegre District, Ribeirão

Preto - SP/ZIP code: 14049-900 Campus address: Rua Pedreira de Freitas, House 01, FMRP/USP, Ribeirão Preto, SP, Brazil. E-mail: assisbaima@usp.br

References

[1] Canale ST. Campbell's operative orthopaedics. 12th edition. Rio de Janeiro, RJ; 2017.

[2] Elias JJ, Frassica FJ and Chao EY. The open section effect in a long bone with a longitudinal defect - a theoretical modeling study. J Biomech 2000; 33: 1517-22.

[3] Weinkamer R, Eberl C and Fratzl P. Mechanoregulation of bone remodeling and healing as inspiration for self-repair in materials. Biomimetics 2019; 4: 1-16.

[4] Chigira M, Watanabe H, Arita S, Noda K, Shimizu T, Shinozaki T and Nagase M. Remodeling of large bone defects in the treatment of space-occupying lesions - Curettage without bone graft for treating benign bone tumors. Arch Orthop Trauma Surg 1992; 111: 61-65.

[5] Hirn M, Silva U, Sidharthan S, Grimer RJ, Abudu A, Tillman RM and Carter SR. Bone defects following curettage do not necessarily need augmentation. Acta Orthop 2009; 80: 4-8.

[6] Puri A and Gulia A. Curettage of benign bone tumors and tumor like lesions: a retrospective analysis. Indian J Orthop 2013; 47: 645-646.

[7] Shears E, Dehne K, Murata H, Abudu A, Grimer RJ, Tillman RM and Carter SR. Healing of ungrafted bone defects of the talus after benign tumour removal. Foot Ankle Surg 2008; 14: 161-165.

[8] Yanagawa T, Watanabe H, Shinozaki T and Takagishi K. Curettage of benign bone tumors without grafts gives sufficient bone strength. Acta Orthop 2009; 80: 9-13.

[9] Federal University of São Paulo. Guide to anesthesia and analgesia in laboratory animals. 2020.

[10] Lima I, Lopes RT, Oliveira LF and Alves JM. Analysis of bone structure through 3D microcomputed tomography. Rev Bras Física Médica 2009; 2: 6-10.

[11] Pessan VJO, Volpon JB and Shimano AC. Mechanical flexural test on the concave and convex faces of the rat femur diaphysis. Rev Bras Ortop 1996; 31: 600-604.

[12] Nemecek E, Chiari C, Valentinitsch A, Kainberger F, Hobusch G, Kolb A, Hirtler L, Trost C, Vukicevic S and Windhager R. Analysis and quantification of bone healing after open wedge high tibial osteotomy. Wien Klin Wochenschr 2019; 131: 587-598.

[13] Mehta M, Heyland M, Toben D and Duda GN. Microstructure and homogeneity of distribution of mineralised struts determine callus strength. Eur Cells Mater 2012; 25: 366-379.

[14] Nyman JS, Munoz S, Jadhav S, Mansour A, Yoshii T, Mundy GR and Gutierrez GE. Quantitative measures of femoral fracture repair in rats derived by micro-computed tomography. J Biomech 2009; 42: 891-897.

[15] Sigurdsen U, Reikeras O, Hoiseth A and Utvag SE. Correlations between strength and quantitative computed tomography measurement of callus mineralization in experimental tibial fractures. Clin Biomech 2011; 26: 95-100.

[16] Fiset S, Godbout C, Crookshank MC, Zdero R, Nauth A and Schemitsch EH. Experimental validation of the radiographic union score for tibial fractures (RUST) using micro-computed tomography scanning and biomechanical testing in an in-vivo rat model. J Bone Joint Surg Am 2018; 100: 1871-1878.

[17] Wright DA, Nam D and Whyne CM. A comparison of stereology, structural rigidity and a novel 3D failure surface analysis method in the assessment of torsional strength and stiffness in a mouse tibia fracture model. J Biomech 2012; 45: 2236-2240.

[18] Shefelbine SJ, Simon U, Claes L, Gold A, Gabet Y, Bab I, Müller R and Augat P. Prediction of fracture callus mechanical properties using micro-CT images and voxel-based finite element analysis. Bone 2005; 36: 480-488.

[19] Baima Filho FAS, Mendonça PG, Silva GEB, Santos OJD, Garcia JBS and Cartagenes MDSS. The analysis of alendronate action in bone fracture healing in rats. J Clin Orthop Trauma 2020; 11 Suppl 5: S856-S860.

[20] Ashman O and Phillips AM. Treatment of nonunions with bone defects: which option and why? Injury 2013; 44 Suppl 1: S43-S45.

[21] Nauth A, Schemitsch E, Norris B, Nollin Z and Watson JT. Critical-size bone defects: is there a consensus for diagnosis and treatment? J Orthop Trauma 2018; 32 Suppl 1: S7-S11.

[22] Roddy E, DeBaun MR, Daoud-Gray A, Yang YP and Gardner MJ. Treatment of critical-sized bone defects: clinical and tissue engineering perspectives. Eur J Orthop Surg Traumatol 2018; 28: 351-362.

[23] Warmke LM, Maloney N, Leung CH, Lin H, Lazar AJ and Wang WL. SATB2 expression in undifferentiated pleomorphic sarcomas of bone. Am J Clin Pathol 2022; 158: 235-241.

[24] Mouillé M, Rio M, Breton S, Piketty ML, Afenjar A, Amiel J, Capri Y, Goldenberg A, Francannet C, Michot C, Mignot C, Perrin L, Quelin C, Van Gils J, Barcia G, Pingault V, Maruani G, Koumakis E and Cormier-Daire V. SATB2-associated syndrome: characterization of skeletal features and of bone fragility in a prospective cohort of 19 patients. Orphanet J Rare Dis 2022; 17: 100.

[25] Zarate YA, Steinraths M, Matthews A, Smith WE, Sun A, Wilson LC, Brain C, Allgove J, Ja-

cobs B, Fish JL, Powell CM, Wasserman WW, van Karnebeek CD, Wakeling EL and Ma NS. Bone health and SATB2-associated syndrome. Clin Genet 2018; 93: 588-594.

[26] Atrash S, Robinson M, Taneja A, Paul B, Cassetta K, Ndiaye A, Varga C, Block J, Lipford EH, Smith ET, McCall CM, Thurston V, Foureau D, Usmani SZ, Voorhees PM and Bhutani M. Bone marrow Ki-67 index is of prognostic value in newly diagnosed multiple myeloma. Eur J Haematol 2023; 111: 373-381.

[27] Chen Y, Liu J, Zhou B, Yang M and Feng H. The value of Ki-67 as a prognostic biomarker in osteosarcoma: a systematic review and meta-analysis. Asian J Surg 2022; 45: 2978-2980.

[28] Hsiao CY, Chen TH, Chu TH, Ting YN, Tsai PJ and Shyu JF. Calcitonin induces bone formation by increasing expression of Wnt10b in osteoclasts in ovariectomy-induced osteoporotic rats. Front Endocrinol (Lausanne) 2020; 11: 613.